Paper submitted to the Winter ASME Meeting, Nov. 27-Dec. 2, 1988, Chicago, IL.

RESPONSE OF MATERIALS TO HIGH HEAT FLUXES DURING OPERATION IN FUSION REACTORS*

A. M. Hassanein
Fusion Power Program, Argonne National Laboratory
9700 S. Cass Ave., Argonne, IL 60439 USA

DISCLAIMER

July 1988

*Work supported by the U. S. Department of Energy/Office of Fusion Energy under contract W-31-109-Eng-38.

RESPONSE OF MATERIALS TO SEVERE HEAT FLUXES DURING OPERATION IN FUSION REACTORS*

A. M. Hassanein
Fusion Power Program
Argonne National Laboratory
9700 S. Cass Ave., Argonne, IL 60439 USA

ABSTRACT

Very high energy deposition on first wall and other components of a fusion reactor is expected due to plasma instabilities during both normal and off-normal operating conditions. Off-normal operating conditions result from plasma disruptions where the plasma loses confinement and dumps its energy on the reactor components. High heat flux may also result from normal operating conditions due to fluctuations in plasma edge conditions. This high energy dump in a short time results in very high surface temperatures and may consequently cause melting and vaporization of these materials. The net erosion rates resulting from melting and vaporization are very important to estimate the lifetime of such components. The response of different candidate materials to this high heat fluxes is determined for different energy densities and deposition times. The analysis used a previously developed model to solve the heat conduction equation in two moving boundaries. One moving boundary is at the surface to account for surface recession due to vaporization and the second moving boundary is to account for the solid-liquid interface inside the material. The calculations are done parametrically for both the expected energy deposited and the deposition time. These ranges of energy and time are based on recent experimental observations in current fusion devices. The candidate materials analyzed are stainless steel, carbon, and tungsten.

INTRODUCTION

Very high heat fluxes on the plasma chamber wall, on limiters/divertor plates and on other components of a fusion reactor are expected during both normal and off-normal operating conditions. Off-normal operating conditions can result from unipolar arcing, run-away electrons, and plasma energy dump following a disruption event. High energy deposition may also result during normal operating conditions because of fluctuations in plasma edge conditions recently known as edge localized modes (ELMS). The energy deposited on these components during such events can be in the order of several hundred megajoules. This high energy deposition time is recently believed to be much less than 1 ms. As a result, the energy on the high heat flux components may reach values up to 10,000 KW/cm^2 or even higher. Severe melting and vaporization of the reactor components may then occur. It is then important to accurately evaluate the amount of material evaporated and melted from the exposed surfaces at these short deposition times. The evaporated material may contaminate the plasma with a high-Z material such as tungsten. But more seriously, both evaporation and melting will contribute to the first wall, limiter, and divertor plate erosion which consequently limits the lifetime of these components and hence the availability of the reactor.

Recent modeling efforts (1-6) have focused on the analysis and on the development of computer codes to quantify the effects of the high energy dump on reactor materials. The analysis presented here used a previously developed model to solve the heat conduction equation with nonlinear boundary conditions (1). In this model the surface temperature is determined by both the boundary conditions as well as by the kinetics of the evaporation process. The kinetics of the evaporation establish the connection between the surface temperature and the net atom flux leaving the surface taking into account the possibility of recondensation. Consequently, this heat conduction problem is highly non-linear and involves two moving boundaries. One moving boundary is at the melt-solid interface, while the other is due to the surface receding as a result of the vaporization losses. Several improvements in calculational methods

* Work supported by the U.S. Department of Energy under contract No. W-31-109-Eng-38.

have recently been incorporated into the analysis. These include advanced numerical methods for more accurate temperature calculation in moving boundaries problems. Both finite difference and finite element methods have been used efficiently to solve this system of equations, and consistent results were obtained (6). Improved analytical expressions for thermophysical properties are used to provide a better fit over a wider temperature range. Numerical results are given for candidate materials such as stainless steel, carbon, and tungsten. These results are given parametrically in terms of the deposition times and energy densities. Short disruption times recently suggested may cause severe erosion rates and may limit reactor component lifetime.

Several experiments have recently been carried out using an electron beam test facility to investigate the consequences of simulated plasma disruption (7-10). The general conclusions from these experiments have indicated a fairly good agreement between the models and the calculations described in this paper and the measured values for the melt layer and vaporization thicknesses.

CALCULATIONAL MODEL

The model used in this analysis is discussed in detail elsewhere (11). Only a brief summary is given below. The general time-dependent one-dimensional heat conduction equation with thermophysical properties κ, ρ, C_p of the material that vary with temperature is given by:

$$\rho_s(T)\, C_{p_s}(T)\, \frac{\partial T_s}{\partial t} = \frac{\partial}{\partial x}\left[K_s(T)\, \frac{\partial T_s}{\partial x}\right] \quad 0\le x\le L,\ t>0 \qquad (1)$$

$$T(x,o) = f(x) \qquad 0\le x\le L,\ t=0 \qquad (2)$$

where $f(x)$ is the initial temperature distribution function. The developed computer code can also handle a volumetric heat generation source term $Q(x,t)$ added to Eq. (1).

The correct boundary condition requires partitioning of the incident energy into conduction, melting, evaporation, and radiation. Thus the total input heat flux $q(t)$:

$$q(t) = q_c + q_v + q_r \qquad (3)$$

where

$$q_c = \text{conduction heat flux} = K(T)\, \frac{\partial T}{\partial x}\Big|_{x=0} \qquad (4)$$

$$q_v = \text{vaporization heat flux} = \rho(T_v)\, L_v\, V(T_v) \qquad (5)$$

$$q_r = \text{radiation heat flux} = \varepsilon\sigma\left(T_v^4 - T_a^4\right) \qquad (6)$$

where $T_v = T(x = 0, t)$ is the surface temperature, L_v is the heat of vaporization. $v(T_v)$ is the velocity of the receding surface, σ is the Stefan-Boltzmann Constant, ε is the emissivity of the target material, and T_a is the ambient temperature of the surface not exposed to the energy dump but in direct line of sight of the exposed surface. Then the boundary condition at the surface can be written as

$$q(t) = -K(T)\, \frac{\partial T}{\partial x}\Big|_{x=0^+} + \rho(T)\, L_v\, v(T_v) + \varepsilon\sigma\left(T_v^4 - T_a^4\right) \qquad (7)$$

Once melting commences, the condensed phases of the wall or target material define two regions: the liquid phase in the region $s(t) \le x \le m(t)$, and the solid phase in the region $x \ge m(t)$. Here, $m(t)$ is the instantaneous position of the melt-solid interface, and $s(t)$ is the instantaneous position of the surface. The boundary condition at the melt-solid interface is now

$$k_s\, \frac{\partial T_s}{\partial x} - k_\ell\, \frac{\partial T_\ell}{\partial x} = \rho\, L_f\, w(t) \qquad \text{at } x = m(t) \qquad (8)$$

where

$$w(t) = \frac{dm}{dt}\ , \qquad (9)$$

is the velocity of the moving interface and L_f is the latent heat of fusion. The subscripts s and ℓ refer to solid and liquid phases respectively. The thermophysical properties of both solid and liquid phases are different and assumed to vary with temperatures by polonominal functions.

There are several ways of accounting for the moving boundary at the surface due to the evaporation of the wall material (6). One way is to introduce a coordinate frame which moves with the receding surface. Hence, in a frame

$$z(t) = x - \int_o^t v(T)\, dt \qquad (10)$$

The surface remains at $z=0$, but the heat conduction equation transforms into

$$\rho C_p\, \frac{\partial T}{\partial t} - \rho C_p v(T)\, \frac{\partial T}{\partial z} = \frac{\partial}{\partial z}\left[K(T)\, \frac{\partial T}{\partial z}\right] \qquad (11)$$

which differs from the original equation by the convective term $\rho C_p v(T)\, \partial T/\partial z$. All boundary conditions retain their original form given above, and only $\partial T/\partial x$ is replaced by $\partial T/\partial z$.

The velocity of the receding surface, i.e., $v(T)$ is a highly non-linear function of temperature. A review of the model used to calculate the evaporation losses is given in Ref. (11-12). In this model, the surface velocity is highly non-linear function of surface temperature and is given by

$$v(T) = 5.8\times10^{-2}\,\frac{\alpha\sqrt{A}\,P_v(T_v)}{\rho(T_v)\sqrt{T_v}}\left[0.8+0.2\,e^{-t/10\,\tau_c}\right] \quad \text{cm/sec} \qquad (12)$$

where

α = sticking probability (≈1)

A = atomic mass number of target material

P_v = vapor pressure of target material (Torr)

τ_c = vapor collision frequency (sec^{-1})

PHASE CHANGE

When the temperature of a node reaches the melting temperature of the material T_m, then this node temperature is fixed until all the heat of fusion is absorbed. Then the temperature of this node is allowed to change. During the phase change the material properties of the node is given by a combined value from both solid and liquid properties according to the ratio of the transformation at this time step.

VAPOR SHIELDING

If a vapor layer from the exposed material of sufficient thickness has been produced during disruption in front of the incoming plasma ions, the ions may be stopped in this layer rather than in the condensed material of the reactor component (1). This is known as self-shielding concept because it tends to shield and protect the reactor components from further intense damage. This model is discussed in detail as first introduced by the author, et al. in Ref. (1). It is believed that the shorter the deposition time the more effective the shielding from the vapor. This is mainly because at short deposition times the vapor accumulation in front of the incoming plasma is very fast and there is not enough time for this vapor to move and leave the damaged area.

ANALYSIS AND RESULTS

Recent analysis and observations of experimental data for plasma disruptions from current fusion machines such as TFTR and JET, have indicated that the deposition time is very short and may be on the order of a fraction of a millisecond (≈ 0.1 ms). This is in contrast to previous assumptions and analysis in which the disruption times were assumed to be in the 10-20 ms range (13-14). Shorter deposition times usually result in very high surface temperatures which lead to more intense vaporization and surface damage. Accordingly, some of the present calculations were carried out to study the effect of such short deposition times and to compare the result to longer deposition times. Energy densities as large as 1400 J/cm^2 were considered in this analysis. These energy densities were assumed to be deposited at a constant rate over the given deposition time. Three materials are considered in this analysis, stainless steel, carbon, and tungsten. Steel and carbon are two of the main candidate materials for structural or limiter components in fusion reactors. Tungsten being a high temperature refractory metal offers a range of properties that makes it unique compared to stainless steel and carbon. The comprehensive A*THERMAL (15) Computer Code is used to evaluate the response and lifetime of these materials. The code was developed in multi-dimensional form to provide analysis of the energy deposition, temperature response, melting and vaporization thicknesses of different materials exposed to different radiation sources such as x-rays, laser, ions and surface heat fluxes or any simultaneous combination of these sources (16-17). Other subsequent effects produced in materials such as displacement production and sputtering erosion can also be calculated by the code.

The surface temperature of stainless steel (SS), carbon (C), and tungsten (W) as a function of time for two energy densities, i.e., 200 and 500 J/cm^2, is shown in Figs. 1 and 2 respectively. The energy deposition time for this case is assumed to be 1 ms. It can be seen that the surface temperature rapidly exceeds the melting temperature of SS (T_m = 1700°K) for both the energy densities, considered. The surface temperature for both SS and C approaches a steady-state value shortly after the deposition starts. The higher the energy density the steeper the temperature rise and the faster the temperature approaches its steady value. For tungsten the temperature rise is not as sharp but in both cases it exceeds the tungsten melting temperature (T_m = 3680°K). The temperature rise for W is much higher for the case of 500 J/cm^2. At the end of the deposition time, the surface temperature drops sharply and the material cools down continuously. The surface velocity, which is the velocity at which the front surface recedes as a result of vaporization, depends on the surface temperature as well as on material properties such as vapor pressure (eqn. 12). The integration of this velocity over the time gives the total amount of material vaporized. A comparison of the surface velocity for the three materials is shown in Fig. 3 for input energy density of 500 J/cm^2 and for 1 ms deposition time. Stainless steel has the highest surface velocity compared to both carbon and tungsten, although it has the lowest surface temperature rise. Tungsten has the highest temperature rise as shown in Fig. 2, but has the lowest surface velocity. This is mainly because stainless steel has the highest vapor pressure among the three materials. It is then expected that stainless steel has much higher vaporization losses than both carbon and tungsten at these conditions.

Figure 4 shows the evolution of the melt layer thickness of stainless steel and tungsten as a function of time for the same deposition conditions of Figs. 3 and 4. It can be seen that tungsten has a larger melt layer thickness than steel. The maximum melting thickness occurs around or slightly after the end of the deposition time. However, the stainless steel melt layer duration, i.e, the total time that liquid is present, is longer than in the tungsten case. Melt layer duration times are important when considering issues such as stability and erosion of the melt layer under different forces existing in the reactor chamber (18).

There are still large uncertainties as to the duration for the energy deposition during plasma disruptions. Recent observations in current tokamak machines

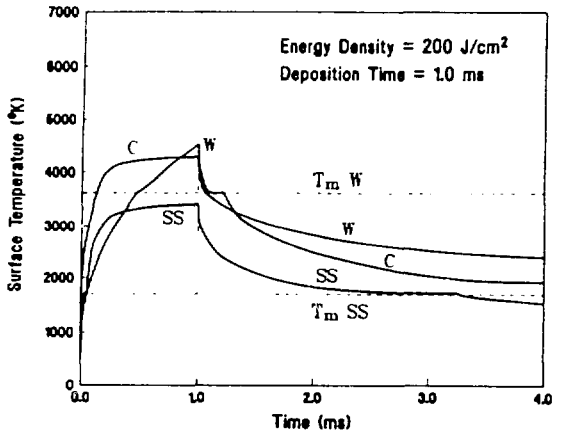

Figure 1
Surface temperature rise as a function of time for different candidate materials.

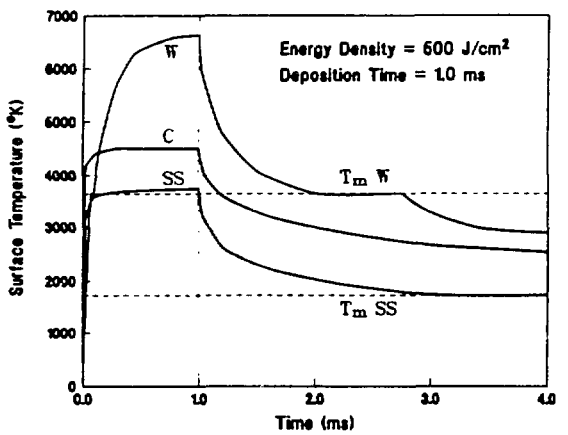

Figure 2
Surface temperature rise as a function of time for different candidate materials.

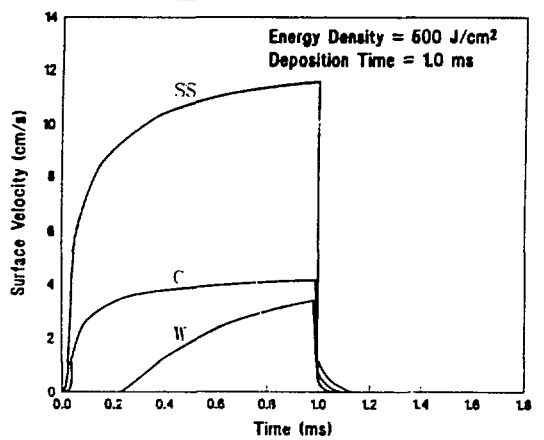

Figure 3
Surface velocity as a function of time for different candidate materials.

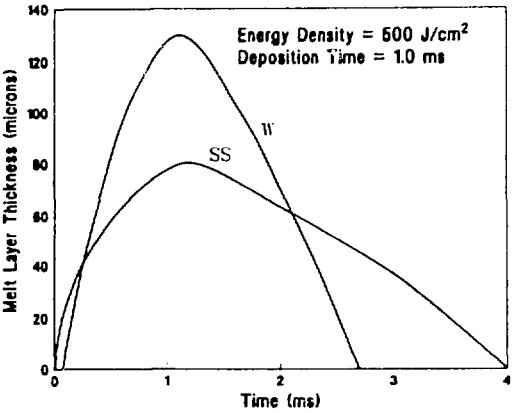

Figure 4
Melt layer thickness as a function of time for stainless steel and tungsten.

suggest that the plasma disruption time may be in the order of a few hundreds of a microsecond. The energy deposition time may be the single most important parameter to determine the net erosion rate from both melting and vaporization and consequently the reactor component lifetime. Figure 5 shows the melt layer thickness of tungsten and stainless steel as a function of the energy deposition time for energy density of 500 J/cm^2. At shorter deposition times the melt layer thickness is small, then it increases with increasing deposition time and then it decreases again. At short deposition times there is not enough time for the deposited energy to be conducted away through the material, rather heating the near surface region to a very high temperature which increases the vaporization losses. Consequently at short deposition times, most of the energy absorbed by vaporization of the surface region. However, at long deposition times most of the energy is conducted through the material away from the surface and the temperature rise is less than that for short deposition times.

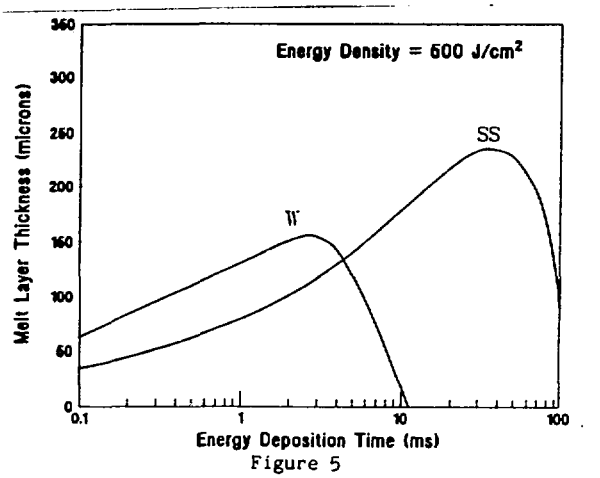

Figure 5
Melt layer thickness as a function of energy deposition time for stainless steel and tungsten.

Figure 6 shows the total melting plus vaporization thickness as a function of the deposition time for the same energy density. For the carbon case only the vaporization thickness is given since carbon does not melt. Vaporization thickness always increases as the deposition time decreases, while for the melt layer there is a specific time where the thickness goes through a maximum, depending on the energy density, type of material, and boundary conditions. If the melt layer is entirely lost at the end of the deposition time then carbon is the best candidate to resist erosion except for energy densities and deposition times where tungsten does not melt. Among the three candidates, stainless steel is the least resistant to erosion under similar conditions.

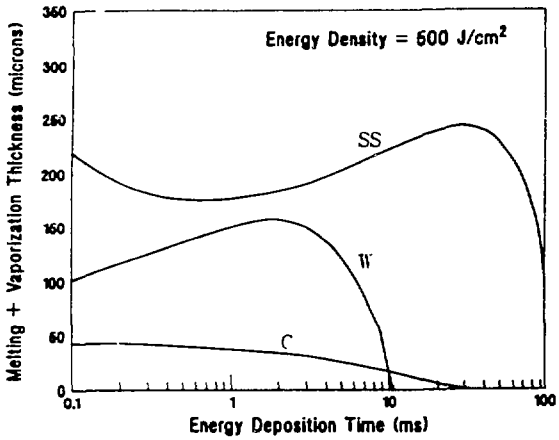

Figure 6
Melting plus vaporization thickness as a function of energy deposition time.

The vaporization and melting layer thicknesses as a function of the deposited energy density are shown in Figs. 7 and 8, respectively. The calculation is done for two deposition times, i.e., 0.1 ms and 10 ms. It is clearly shown in Fig. 7 that longer deposition times substantially reduce the vaporization thickness, especially at lower energy densities. Higher energy densities always increase the total erosion thickness from vaporization for any deposition time. For an energy density of 1400 J/cm^2 and a 0.1 ms deposition time the vaporization thickness from stainless can be as high as 1 mm per disruption. As shown in Fig. 8, the melt layer thickness significantly increases with increasing deposition energy for the longer deposition time (10 ms). However, the melt layer thickness is insensitive to deposition energy for this shorter deposition time (0.1 ms). Again, this is because at short deposition times most of the energy deposited is used in heating the surface to a very high temperature thus causing more surface vaporization and consequently less energy is left to be conducted and produce melting.

The influence of vapor shielding has been examined further. Under certain conditions, vaporized material produced in the early phases of a disruption is expected to partially shield the wall/plate during the remainder of the disruption. This is because the incoming plasma ions will be stopped in the vapor rather than in the

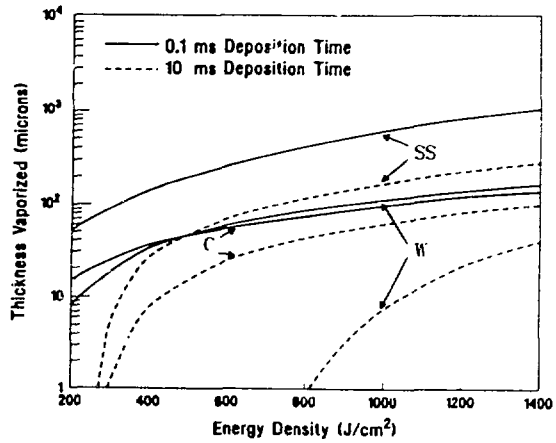

Figure 7
Vaporization thickness as a function of energy density for different candidate materials.

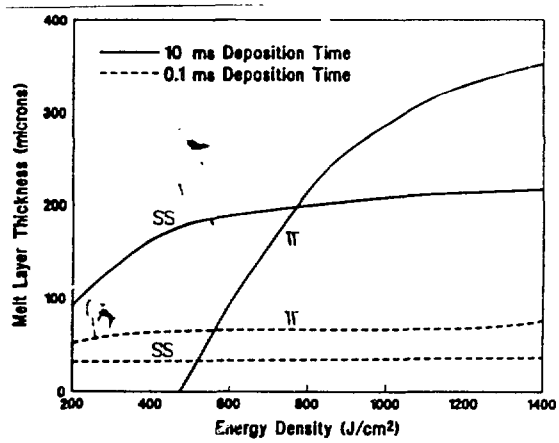

Figure 8
Melt layer thickness as a function of energy density for stainless steel and tungsten.

condensed phase of the wall material. The vapor layer will be heated by the further incoming plasma ions and then reradiate its energy isotropically rather than the incident unidirectional energy flux. As a result, the total energy deposited on the wall, and hence, the subsequent vaporization is significantly reduced. Vapor shielding is expected to be more effective for shorter (~ 0.1 ms) disruption times. The general configuration is also believed to be important. For example, in the divertor region the vaporized material is better confined than in the large plasma chamber, and hence, vapor shielding is expected to be more effective in the divertor region. Figure 9 shows the vaporization thickness as a function of the energy density with and without the effect of vapor shielding for a deposition time of 10 ms. At lower energy densities and longer disruption times the model predicts that vapor shielding reduces vaporization thickness more than at higher energy densities and shorter disruption times. However, as mentioned above, vapor shielding is expected to be

effective mainly at very short deposition times. The effect of vapor shielding on melt layer thickness depends on both the energy deposited and the deposition time. At higher energy deposition and shorter disruption times, where most of the deposited energy is used in vaporizing the surface, vapor shielding is not expected to change the melt layer thickness by a wide margin. In most cases vapor shielding slightly reduces the melt layer thickness and in a few cases it may slightly increase the melt layer thickness. Only near the threshold energies for melting where vapor shielding is expected to have a large impact on the melt layer thickness.

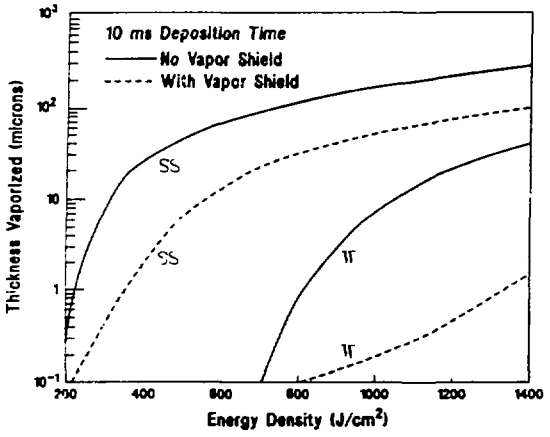

Figure 9
Vaporization thickness with and without the effect of vapor shielding.

CONCLUSIONS

Parametric analysis of the erosion rates from melting and vaporization were done for candidate fusion materials. This analysis reflects the experimental observation from the current tokamak machines for both the expected energy being deposited and the deposition time. High energy densities and short disruption times can severely hinder the successful operation of fusion reactors and sharply limit its lifetime. An accurate estimation of the disruption time, energy, and the area of deposition is very important in determining material erosion. The effectiveness of vapor shielding and the stability of melt layer formation in a strong magnetic field environment are also very important factors in determining the total material loss during a disruption.

BIBLIOGRAPHIC REFERENCES

1. A.M. Hassanein, G.L. Kulcinski, and W.G. Wolfer, J. Nucl. Mat., 103&104 (1981) 321.

2. B.J. Merrill and J.L. Jones, "Modeling the Thermodynamic Response of Metallic First Walls During a Plasma Disruption," J. Nucl. Mater., 111/112 (1982) 544.

3. R.R. Peterson, "Radioactive Heat Transfer in Self-Shielding Vapor Layer During Tokamak Disruptions," University of Wisconsin Report, UWFDM 537 (1983).

4. S. Murray and G. Bronner, "Disruption Model," Princeton Plasma Physics Laboratory Report, PPPL 1909 (1982).

5. H. Hashizume et al., Fusion Engr. and Design, 5 (1987) 141.

6. A. Hassanein, to be published.

7. J.R. Easoz and R. Bajaj, Proc. 10th Symp. of Fusion Engineering (1983).

8. C.D. Croessmann, G.L. Kulcinski, and J.B. Whitley, J. Nucl. Mater., 128/129 (1984) 816.

9. M. Seki et al., J. Fusion Energy, 5 (1986) 181.

10. F. Brossa et al., J. Nucl. Mat., 141-143 (1986) 210.

11. A.M. Hassanein, G.L. Kulcinski, and W.G. Wolfer, Nucl. Engr. and Design/Fusion, 1 (1984) 307.

12. A.M. Hassanein, J. Nucl. Mat., 122&123 (1984) 1453.

13. INTOR, Zero phase, Intern. Atomic Energy Agency, Vienna (1980).

14. C.C. Baker et al., "STARFIRE - A Commercial Tokamak Fusion Power Plant Study," Argonne National Laboratory Report, ANL/FPP/80-1 (1980).

15. A.M. Hassanein, "Modeling the Interaction of High Power Ion or Electron Beams with Solid Materials," ANL/FPP/TM-179 (1983).

16. A.M. Hassanein, J. Nucl. Mater., 122&123 (1984) 1459.

17. A.M. Hassanein, H.M. Attaya, and G.L. Kulcinski, J. Nucl. Mater., 141-143 (1986) 221.

18. W.G. Wolfer and A.M. Hassanein, J. Nucl. Mater., 111&112 (1982) 560.